Academic Journal of Science and Technology
ISSN: 2771-3032 | Vol. 5, No. 1, 2023

Two-parameter Optical Sensing Based on Multilayer Parity-time-symmetric Structure

Xunqiang Huang, Ziming Meng*

College of Physics and Optoelectronic Engineering, Guangdong University of Technology, Guangzhou, Guangdong 510006, China

Abstract: A two-parameter sensor that can detect the variation of temperature and refractive index is realized in a multilayer dielectric structure obeying parity-time (PT) symmetry. The sensor can operate near exceptional points (EPs), which have been shown to provide dramatic variations of their eigenvalues in response to small parameter changes. The optical sensing behavior is theoretically investigated based on the transfer matrix method. The results show that the sensor can work within the surrounding temperature (t_p) ranging from 0 to 30℃, and the refractive index (n_g) of incident medium ranging from 1.0 to 1.4. The minimum detectable variation $\triangle n_{g,min}$ of the sensor can reach 0.02. The sensitivity of n_g and t_p can reach 372496.53 RIU^{-1} and 249.18$℃^{-1}$, respectively. Our structures show great promise in temperature monitoring in cold environment and identification of chemical gases or liquids.

Keywords: Parity-time-symmetric system, Exceptional point, Temperature monitoring, Refractive monitoring.

1. Introduction

The paraxial approximation of the electromagnetic field propagation equation and the Schrodinger equation are similar in mathematical form, even though they have different origins. This similarity provides a platform for studying PT symmetry and non-Hermiticity in optical systems. It is known that the non-Hermitian operators satisfying PT symmetry can have real eigenvalue similar to Hermitian operators which is first proposed by Bender et al [1-3]. The PT-symmetric non-Hermitian systems have an exceptional point (EP). EP is phase transition point between the PT-symmetric and the PT-symmetric broken phase. The sensor operating near EP, which have been shown to provide dramatic variations of their eigenvalues in response to small parameter changes. The peculiar optical phenomena near EP have important applications in optical super-sensitive detector [4,5], unidirectional reflectionless propagation [6], waveguide transmission [7], gas sensing [8], particle and biological sensing [9-12] etc. The application of EP phenomenon in PT symmetry system in optical field has great development prospects. However, it is difficult to adjust the sensitive response range of previous optical sensors operating near EP. Multiple small parameter changes cannot be measured neither. Ref [13] proposed a two-parameter optical fiber sensor. However, the miniaturization and integration of optical fiber sensors cannot be well realized. Some sensors with good performance and capable of measuring two-parameters have been reported [14-16]. But the sensitive range of sensor cannot be adjusted on demand, which is difficult to use in different occasions of sensing.

In this work, a two-parameter sensor built in a multilayer dielectric structure obeying PT symmetry is theoretically investigated for realizing highly sensitive temperature and refractive index detection. Transfer matrix method is used to obtain the optical response of our structures. EP in PT system can be realized by the adjustment of structure parameter. The abrupt 2π phase transition is found to verify the existence of the EP. The sensitive response range of the sensor can be adjusted, so it can achieve high sensitivity in the specified range of different parameters. Thus, the structure show great promise in temperature monitoring in cold environments and identification of chemical gases or liquids.

2. Model and Method

PT-symmetric multilayer structure is constructed by using low refractive index material (A layer), silicon film (B layer), gain film (G layer), loss film (L layer), and polydimethylsiloxane (PDMS) material (C layer) This multilayer structure also be called a quasi photonic crystal. The schematics of our structure is shown in Fig.1. It is worth mentioning that the structure was not designed with a metal film layer. Thus, the real part of the refractive index (RI) of the system is a even function and the imaginary part of the RI is an odd function, so the sensor is a strictly PT-symmetric structure.

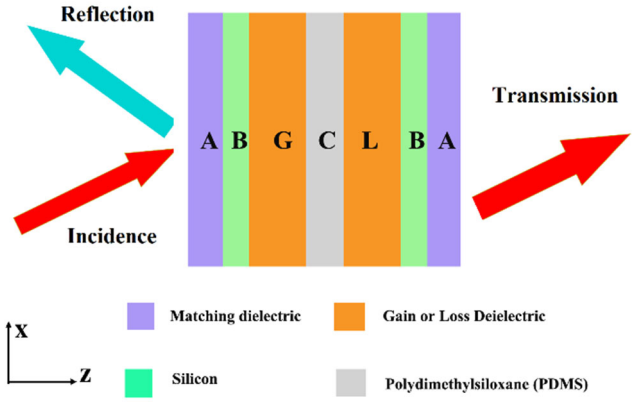

Figure 1. Multilayer PT-symmetric sensor

For the layer A, B, C, G and L layers, the thicknesses and RI of dielectrics are d_A=112.07 nm, n_A=0.45; d_B=47.51 nm, n_B=3.42; dc=114.63 nm and d_G=d_L=135.42 nm, n_G=1.17-iτ and n_L=1.17+iτ, respectively. It should be noticed that the RI of C layer n_c changes with the temperature(t_p), meeting the following formula [17]:

$$n_C = -4.5\times10^{-4}\times t_p + 1.4176, \quad (5)$$

where t_p represents the surrounding temperature. The layer A with low refractive index can be prepared from artificially low refractive index metamaterials [19,20]. The reason for using such a low RI layer is to narrow the linewidth of transmission spectrum, which is beneficial to realize sensitive sensing performance. What's more, the G and L layers can be prepared by polymethylhydrosiloxane (PMHS) material in pratice[18].

By adjusting the gain and loss coefficient τ, the structure can reach the PT symmetry and broken phase point (nearby EP). The tiny changes of temperature (t_p) and refractive index of incident medium (n_g) would lead to dramatic change of transmission triggering the detection operation. By precise tuning τ, the sensing sensitivity range of the sensor can change, so its sensing sensitivity is adjusted as needed.

We use the transfer matrix method (TMM) [21,22] to calculate the transmission or reflectance. The transmission matrix of layer k can be written as:

$$M_k = \begin{bmatrix} \cos\delta_k & -\frac{i}{q_k}\sin\delta_k \\ -iq_k\sin\delta_k & \cos\delta_k \end{bmatrix} \quad (1)$$

where $\delta_k = \frac{2\pi}{\lambda_0} n_k h_k \cos\theta_k$ nk,, hk.and $\cos\theta_k$ represent the refractive index, thickness and incident angle of each layer. For TE and TM waves, q_k is $\sqrt{\frac{\varepsilon_0}{\mu_0}} n_k \cos\theta_k$ and $\sqrt{\frac{\varepsilon_0}{\mu_0}}\frac{n_k}{\cos\theta_k}$ respectively, where ε_0 and μ_0 represent vacuum dielectric constant and vacuum permeability, respectively.

The total matrix M (with elements m_{11}, m_{12}, m_{21}, m_{22})of dielectric multilayer can be expressed by the multiplication of matrix M_k of each layer:

$$M\begin{bmatrix} m_{11} & m_{12} \\ m_{21} & m_{22} \end{bmatrix} = \prod_k M_k \quad (2)$$

Then the reflection coefficient r and transmission coefficient t can be expressed as:

$$r = \frac{(m_{11}+m_{12}q_{sub})q_0 - (m_{11}+m_{12}q_{sub})}{(m_{11}+m_{12}q_{sub})q_0 + (m_{11}+m_{12}q_{sub})}, \quad (3)$$

$$t = \frac{2q_0}{(m_{11}+m_{12}q_{sub})q_0 + (m_{11}+m_{12}q_{sub})}, \quad (4)$$

where q_0 and q_{sub} represent the coupling parameters of the covering layer and the structural layer. Therefore, reflectivity and transmittance can be expressed as $R = |r|^2$ and $T = \frac{q_{sub}}{q_0}|t|^2$.

The transmission spectrum of the sensor (Fig. 2) is simulated by TMM and finite element method (FEM), and the results are nearly consistent, which indicates the reliability of the TMM calculation method. Two transmission peaks are found, which originate from the resonance frequency in the two weak cavities ABG and LBA (see the RI difference between layer A, B, G, L). The peak transmission value is T=0.93 (527.91 nm) and T=0.89 (715.60 nm) and the full width at half maximum (FWHM) of two peaks are 7.18 nm and 17.36 nm, respectively.

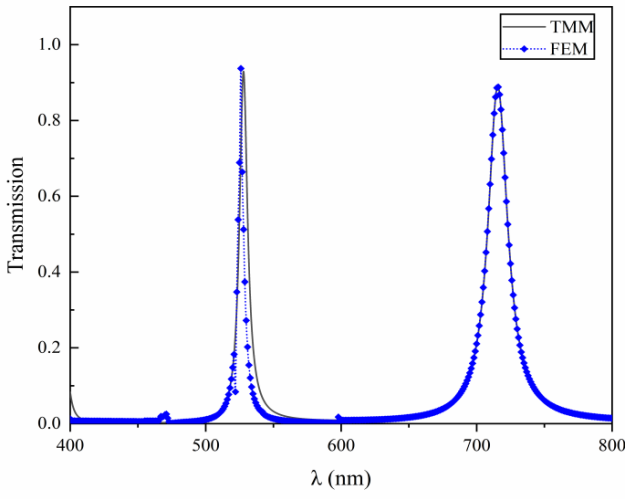

Figure 2. Transmission spectrum of the sensor.

In Fig. 3, the dependence of transmission spectra on τ is presented. When τ=0.053 (nearby EP), there is a stronger enhancement of the maximum of the transmission peak. The peculiar phenomenon can be explained by the enhancement of pole effect by EP [23]. Perturbation of the sensor by the external environment can affect the transmission value as well as the position of the peak (see next section).

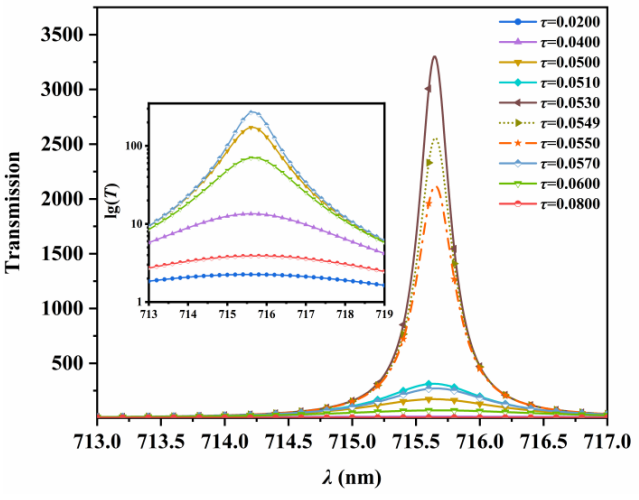

Figure 3. Transmission spectra of sensors with different τ.

3. Results and Analysis

To verify the presence of EP, the phase change at some particular τ is extracted [24,25]. The phase angles φ_t of transmission coefficients t is calculated by TMM. As shown

in Fig. 4(a), when τ equals to 0.00 or 0.02, φ_t does not show negative to positive phase shift (or vice versa). With the increase of τ, the slope of φ_t increases. Fig. 4 (b) shows that when τ equals to 0.053, φ_t jumps from plus $\pi/2$ to minus $\pi/2$ near 716 nm abruptly. Fig.4 (c) indicates that when τ deviates from 0.053, the phase φ_t change becomes gentler. Further increasing τ, the positive to negative phase transition (or vice versa) vanishes as shown Fig. 4(d). So, the sensor works near the EP (τ=0.053) can reach a high sensitivity

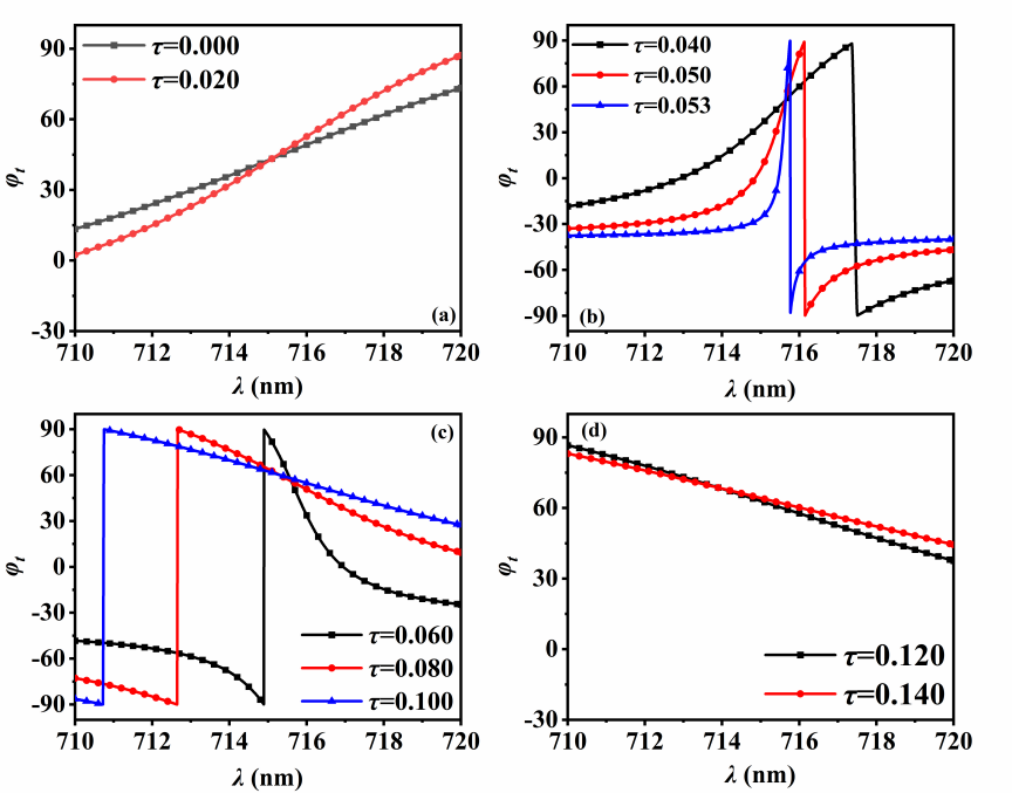

Figure 4. Phase angle φ_t of transmission coefficient on wavelength for different τ.

The small changes lead to significant shifts in the transmission spectrum of the sensor. So, the sensing sensitivity of n_g and t_p are defined as follows [26]:

$$S_1 = -\frac{\Delta T_m}{\Delta t_p}, \tag{6}$$

$$S_2 = -\frac{\Delta T_m}{\Delta n_g}, \tag{7}$$

where ΔT_m, Δt_p, Δn_g are the change of the maximum value of transmission, the change of the temperature of layer C and the change of the refractive index of the incident medium.

The dependence of transmission on t_p from 0 to 100℃($n_g = 1.0$) is shown in Fig. 5 (a). From 0 to 100℃, the shift of peak wavelength $d\lambda$ is about 0.34 nm for Δt_p equaling to 20℃. Ranging from 0 ℃ to 100 ℃, ΔT_m reaches the maximum. As shown in Fig. 6 (a), the sensor sensitivity (S_1) could reach the maximum 249.18 $℃^{-1}$ when t_p=2 ℃ and n_g=1.0. For t_p =30 ℃, S_1 decreases to 32.37 $℃^{-1}$. The sensor can be effectively applied to temperature monitoring in cold environments.

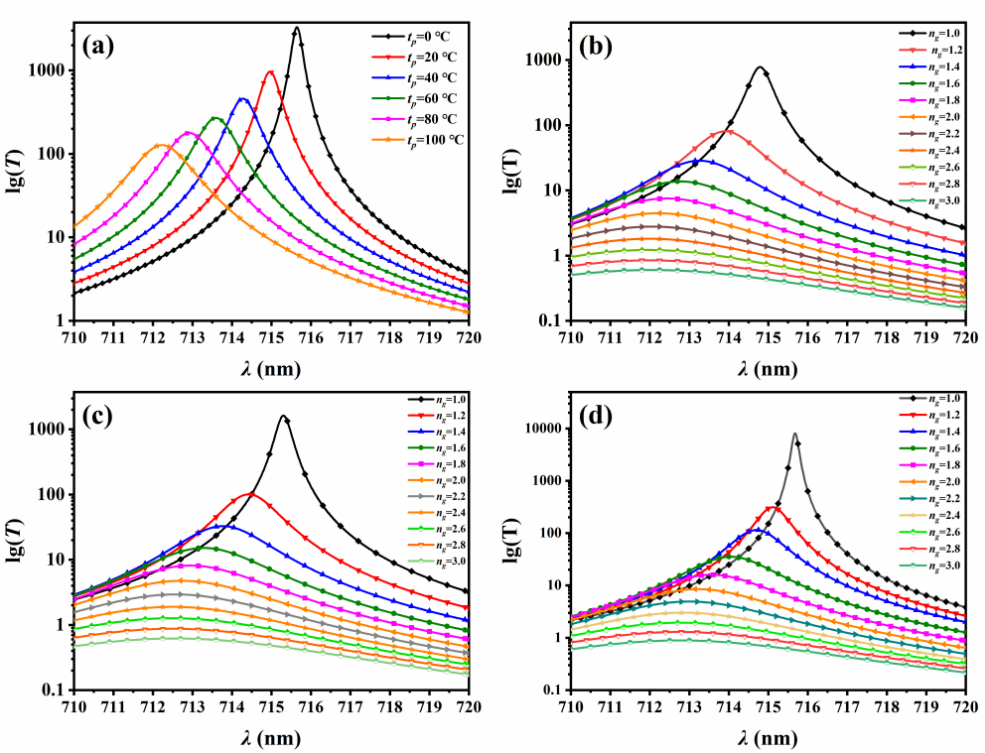

Figure 5. (a) When n_g=1, the transmission spectra of the structure at different temperatures. Dependence of transmission spectra of the structure on incident media at 25℃ (b), 10℃ (c) and 2℃ (d).

The sensor also exhibits a stronger response when changing different incident media. Dependence of transmission lg(T) on n_g when temperature t_p=25℃, 10℃ and 2℃ is shown in Fig.5 (b), (c), (d), respectively. When n_g ranging from 0.95 to 1.40, S_2 can reach the maximum 13287.25 RIU^{-1} on n_g=0.98 (Fig. 6(b)). Besides, the structure distinguishes the minimum refractive index difference of incident media is $\Delta n_{g,min} \approx 0.02$ (see Fig. 6(a)). So, the sensor can be effectively applied in sensing chemical gas or liquid species at low concentrations.

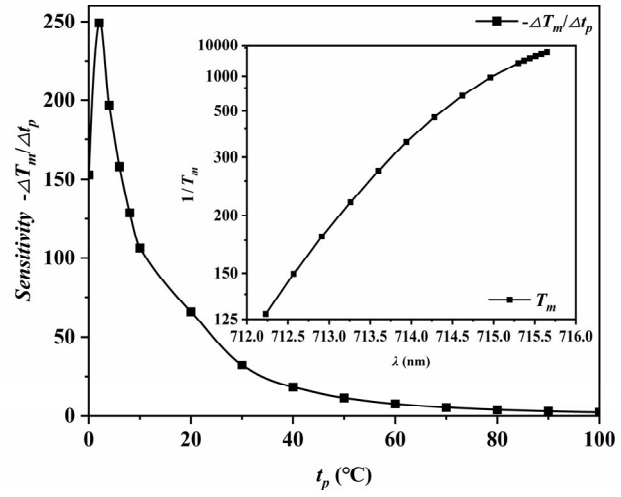

Fig.6 (a)

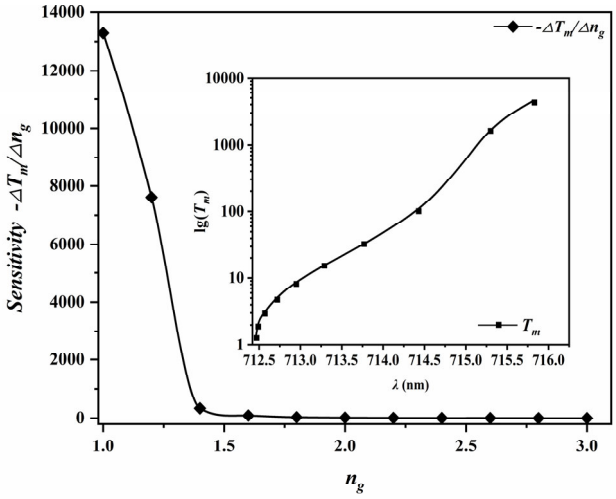

Fig.6 (b)

Figure 6. (a) For n_g=1.0, the dependence of S_1 on t_p. (b) For t_p=10℃, the dependence of S_2 on n_g.

The contour of -$\Delta T_m/\Delta n_g$ *and* -$\Delta T_m/\Delta t_p$ on t_p and n_g when unchanging t_p while varying n_g (ranging from 1.0-3.0 in steps of 0.2) and unchanging n_g while varying t_p (ranging from 0°C to 100°C in steps of 10°C) is shown in Fig. 7(a) and (b), respectively. Contrasting the parameter space of t_p and n_g, S_2 can reach 372496.53 RIU^{-1} on t_p=0℃. The sensor shows strong sensing performance for the t_p ranging from 0°C to 30°C andn_g ranging from 1.0 to 1.4. Besides, the shift of the

transmission peak starts from λ = 716.00 nm (in Fig. 5), which is the existence of the EP. By adjusting τ to change the status of the sensor (such as near EP or away from EP) and thus tune the sensitive sensing range of the sensor.

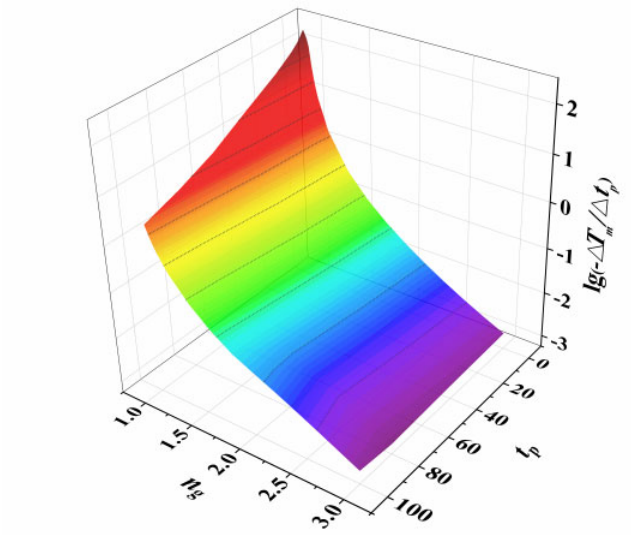

Fig.7 (a)

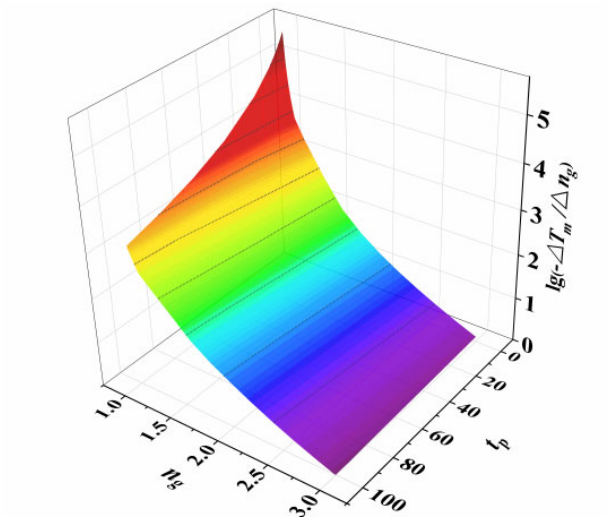

Fig.7 (a)

Figure 7. The parameter space of t_p and n_g with respect to sensitivity lg(-$\Delta T_m/\Delta n_g$). (b) The parameter space of t_p and n_g with respect to sensitivity lg(-$\Delta T_m/\Delta t_p$).

At last, the possible fabrication methods of the sensors are briefly discussed. As a multilayer structure, this sensor can be fabricated easily by layer deposition process such as vapor deposition [27] or sputtering [28], avoiding the need for complicated and costly nanofabrication. The G and L layers can be prepared by PMHS material in practice[18].

4. Conclusion

A two-parameter sensor that can detect the variation of temperature and refractive index is realized in a multilayer dielectric structure obeying PT symmetry. The minimum detectable variation $\triangle n_{g,min}$ of the sensor can reach 0.02. Refractive index sensitivity S_2 can reach 372496.53 RIU^{-1} by contrasting the parameter space of t_p and n_g. The sensor working near the EP (τ=0.053) can reach a high sensitivity. By adjusting τ, we can tune the sensitive sensing range of the sensor. Additionally, the sensor can be fabricated easily by layer deposition process such as vapor deposition [27] or sputtering [28]. And it is suitable for temperature monitoring in cold environment and identification of chemical gases or liquids.

5. Author Profiles

Huang Xunqiang is currently studying for a master's degree at Guangdong Institute of technology. His research interests include theoretical studies on non erlmi optical systems and design of micro - and nano optical sensors.

Meng Ziming received his PhD in optical physics from the Institute of physics, Chinese Academy of Sciences in 2012. In July 2012, he became a postdoctoral fellow at the College of physics and photoelectric engineering, Guangdong Institute of technology. He is currently an associate professor at College of physics and photoelectric engineering, Guangdong Institute of technology. His current research interests include nanophotonics, photonic crystals, plasmonics, ultrafast all-optical switches, and integrated optics.

References

[1] Bender C. M. and Boettcher S. Real spectra in non-Hermitian Hamiltonians having PT-symmetry[J]. Phys. Rev. Lett., 1998, 80(24):5243-5246.

[2] Berry M. V. Physics of non-hermitian degeneracies[J]. Czech. J. Phys., 2004, 54(10):1039-1047.

[3] Rotter I. A non-Hermitian Hamilton operator and the physics of open quantum systems[J]. J. Phys. A: Math. Theor. 2009, 42(15):153001.

[4] El-Ganainy R. et al. The dawn of non-Hermitian optics[J]. Commun. Phys. 2019, 2(37).

[5] Khanbekyan M. and Scheel S. Enantiomer-discriminating sensing using optical cavities at exceptional points[J]. Phys. Rev. A. 2022, 105(5):053711.

[6] Wu Z. L. et al. High-contrast tunable unidirectional reflectionless phenomenon near the exceptional points in integrated bulk Dirac semimetal waveguide[J]. Appl. Phys. Express. 2021, 14(9):094006.

[7] Moiseyev N. and Sindelka M. Transfer of information through waveguides near an exceptional point[J]. Phys.I Rev. A 2021, 103(3):033518.

[8] Nie P. et al. Gas sensing near exceptional points[J]. J. Phys. D. 2021, 54(25):254001.

[9] Gong Z. H. et al. Light-Controlled Exceptional Point Sensor Based on Azo-Functionalized Whispering Gallery Mode Microcavity[J]. IEEE. Sensors J. 2022, 22(11):10485-10491.

[10] Wang Z. J. et al. Dominated mode switching and nanoparticle detection at exceptional points[J]. J Opt. Soc. A. B. 2023, 40(1):108-114.

[11] Chen P. Y. and Jung J. PT-symmetry and Singularity-Enhanced Sensing Based on Photoexcited Graphene Metasurfaces[J]. Phys. Rev. Appl. 2016, 5(6): 064018.

[12] Liu Y. et al. Biosensing Near the Exceptional Point Based on Resonant Optical Tunneling Effect[J]. Micromachines. 2021, 12(4):426

[13] Yin Z. Y. et al. Refractive index and temperature dual parameter sensor based on a twin-core photonic crystal fiber[J]. J. Phys. D: Appl. Phys. 2022, 55(15):15510.

[14] Guo Q. et al. Femtosecond Laser Inscribed Sapphire Fiber Bragg Grating for High Temperature and Strain Sensing[J]. IEEE. 2019, 18(18): 208-211.

[15] Jia P. G. et al. Batch-producible MEMS fiber-optic Fabry-Perot pressure sensor for high-temperature application[J]. Applied Optics. 2018, 57(23):6687.

[16] Jieun Y, et al. Non-Hermitian heterostructure for two-parameter sensing[J]. Opt. Lett. 44(7):1626.

[17] Zhu Z. et al. Surface-plasmonresonance-based optical-fiber temperature sensor with high sensitivity and high figure of merit[J]. Opt. Lett. 2017, 42(15):2948–51.

[18] Yuan Y. et al. Hydrophobic, ultra-low refractive index films prepared by sol-gel process[J]. Mater. lett. 2016, 184(DEC.1):305-307.

[19] Xiao Z. G. et al. Microwave antenna based on low refractive index medium, High Power Laser and Particle Beams[J]. 2014, 26(1):174-178.

[20] Stefan E. et al. A Metamaterial for Directive Emission[J]. Phy. Rev. Lett. 2002, 89(21):213902.

[21] Katsidis C C. et al. General transfer-matrix method for optical multilayer systems with coherent, partially coherent, and incoherent interference[J]. Applied Optics. 2002, 41 (19): 3978-87.

[22] Hawkes J J. et al. Single half-wavelength ultrasonic particle filter: Predictions of the transfer matrix multilayer resonator model and experimental filtration results[J]. The Journal of the Acoustical Society of America. 2002, 111(3):1259.

[23] Fang Y. T. et al. Sensing Gases by the Pole Effect of Parity-Time Symmetric Coupled Resonators[J]. IEEE SENS J. 2018, PP(7):1-1.

[24] Liu F. M. et al. Exceptional Points in Non-Hermitian Photonic Crystals Incorporated With a Defect[J]. Appl. Sci. 2020, 10(3):823.

[25] Dong Z. et al. Large lateral shift in complex dielectric multilayers with nearly parity–time symmetry[J]. Opt. Quant. Electron. 2018, 50(8):323.

[26] Ma R. k., Xia J., and Fang Y. T. Singular pole and enhanced sensitivity of PT-symmetric layered structure with resonators[J]. Eur. Phys. J. Appl. Phys. 2018, 84(1): 10503.

[27] Priya M., Ahmed .A and Karen K. G., Vapor deposition routes to conformal polymer thin films[J]. Beilstein J. Nanotechnol. 2017, 8(76):723.

[28] Smentkowski V. S. Trends in sputtering[J]. Prog. Surf. Sci. 2000, 64(1-2):1-5.